Nature Communications

https://doi.org/10.1038/s41467-026-70100-3

Article in Press

Stratospheric precursor induces wintertime phase reversal of the "warm Arctic-cold Eurasia" pattern

Received: 15 September 2025

Accepted: 18 February 2026

Cite this article as: Zhang, Y., Yin, Z., Tian, W. *et al.* Stratospheric precursor induces wintertime phase reversal of the "warm Arctic-cold Eurasia" pattern. *Nat Commun* (2026). https://doi.org/10.1038/s41467-026-70100-3

Yijia Zhang, Zhicong Yin, Wenshou Tian, Shengping He & Pangchi Hsu

Stratospheric precursor induces wintertime phase reversal of the "Warm Arctic-Cold Eurasia" pattern

Yijia Zhang[1,2]#, Zhicong Yin[1,2,]*#, Wenshou Tian[3], Shengping He[4], Pangchi Hsu[1,2]

[1]State Key Laboratory of Climate System Prediction and Risk Management, Nanjing University of Information Science and Technology; Nanjing, China

[2]School of Atmospheric Sciences, Nanjing University of Information Science and Technology; Nanjing, China

[3]Key Laboratory for Semi-Arid Climate Change of the Ministry of Education, College of Atmospheric Sciences, Lanzhou University; Lanzhou, China

[4]Geophysical Institute, University of Bergen and Bjerknes Centre for Climate Research; Bergen, Norway

*Corresponding author: Zhicong Yin, Email (yinzhc@nuist.edu.cn).

#These authors contributed equally to this work: Yijia Zhang, Zhicong Yin

Abstract

Rapid Arctic warming has reached 2–4 times the global average, contrasting with the cooling trend in mid-high latitude Eurasia during the 1990s–2010s. A notable phenomenon of this so-called "warm Arctic-cold Eurasia" (WACE) pattern is its frequent phase reversal between early and late winter seen in the last decade. As one of the important drivers of climate variability, the role of the stratosphere in WACE reversal remains unclear. Here, we find that approximately 25 days before WACE reversal, the morphology of the stratospheric polar vortex over North America-North Atlantic undergoes a transition between stretching and contraction. Through vertical wave coupling and downward propagation, this stratospheric transition effectively modulates the key atmospheric circulation responsible for the WACE reversal. CMIP6 models including complete stratospheric processes can successfully simulate the WACE reversal induced by the stratospheric precursor, while low-top models fail to capture this linkage. Our findings deepen the understanding of cold-warm transition events from a stratosphere-troposphere coupling perspective.

Introduction

The seesaw linkages between Arctic and Eurasian winter temperatures have garnered considerable attention[1-3]. Explorations mainly focus on both the long-term trend of "Arctic warming-Eurasia cooling" and the interannual-decadal variability of the "warm Arctic-cold Eurasia" (WACE) pattern[4-5]. In the recent decade, a notable phenomenon of WACE pattern is its frequent phase reversal between early and late winter[6]. That is to say, a significant reversal between WACE phase and "cold Arctic-warm Eurasia" (CAWE) phase occurs in a single winter, and the phase in both early and late winter is pronounced and persistent (Supplementary Fig. 1). Such phase reversal was observed in seven winters since 2012, indicating a notable increase in subseasonal variability. The opposite anomalies between early and late winter cancel each other out on the winter-mean scale, thus presenting a weakened "Arctic warming-Eurasia cooling" trend[6,7]. The WACE reversal causes a dramatic change in the meridional gradient of surface air temperature (SAT) between Arctic and Eurasia[8], and substantially enhances the likelihood of extreme events, including the winter abrupt cold-warm transition in East Asia and the severe spring super sandstorms in North China[9,10]. Understanding the physical processes and mechanisms underlying the

WACE reversal is therefore essential for interpreting Arctic-Eurasia climate variability and its implications for extreme climate.

The formation mechanisms of the WACE pattern have been widely discussed, with more insights revealed on the interannual-decadal scales. Climate forcing factors, such as the autumn Arctic sea ice melting[11,1], La Niña[13], and the Pacific Decadal Oscillation[14], can contribute to the WACE pattern through Rossby wave and stratosphere-troposphere interactions. In the atmospheric internal variability, the weakened stratospheric polar vortex and the deep Arctic warming are also conducive to the formation of the WACE pattern[15,16]. In recent years, increasing attention has been devoted to the phase reversal of WACE between early and late winter, and its underlying physical mechanisms are being progressively uncovered. The coordination of the preceding tropical-subtropical sea surface temperature anomalies in the North Atlantic and Indian Ocean can effectively modulate the reversal between the WACE and CAWE phase[6]. In addition, the reversal of Ural blocking anomalies in late December is also a potential factor, which can affect the upward propagation of planetary-scale waves to promote the contribution of stratospheric polar vortex to the SAT reversal in Arctic-Eurasia regions[17]. Previous studies provided physical explanations for the WACE reversal by focusing on the air-sea interaction and the variations of tropospheric atmospheric circulations. However, as a key driver of extreme climate, it remains unclear whether the stratospheric variability can impact the phase reversal of the WACE pattern between early and late winter.

The stratospheric polar vortex (SPV) is a critical bridge linking the stratospheric variability and the tropospheric response, and plays a crucial role in climate changes over the mid-high latitudes[18,19]. The SPV anomalies can affect the phase of Arctic Oscillation/North Atlantic Oscillation (NAO) through various mechanisms such as downward propagation of zonal-mean anomalies, vertical wave coupling, surface amplification[20,21], thereby modulating the frequency of tropospheric blockings in the North Atlantic-Eurasia and the intensity of East Asian winter monsoons[22,23]. The weakened SPV contributes to an increasing number of cold air outbreaks in the Northern Hemisphere, especially over northern Eurasia and eastern America[24,25]. A stretched SPV, characterized by zonally asymmetric anomalies, can also lead to cold anomalies over Eurasia through stratosphere-troposphere coupling[26,27]. The stratosphere exhibits a longer characteristic timescale compared to the troposphere, thus serving as an important source of

subseasonal-seasonal predictability for the extreme climate[28,29]. In several winters, the SPV undergoes a significant phase transition, such as the 1987/1988 winter. The SPV exhibited a prominent transition from weak to strong, accompanied by an out-of-phase tropospheric zonal wind anomaly between early and late winter[30]. This suggests that the changes in the strength or morphology of the SPV have a potential effect on the SAT reversal in the Arctic-Eurasia region, although this mechanism has not yet been revealed.

Given the close linkages between SPV and troposphere-surface climate variability, we propose exploring the role of the stratosphere in the WACE reversal. We first examine the characteristics and lead time of the SPV associated with the WACE reversal, and then investigate the pivotal processes by which the SPV modulates the phase reversal between WACE and CAWE. The key linkages and processes proposed are further demonstrated in the large ensemble simulations, and the reasons for the differences in simulation abilities are discussed.

Results

Linkages between SPV morphology transition and WACE reversal

The WACE pattern is usually expressed by the SAT difference between the Barents–Kara seas (70°–85°N, 30°–100°E) and Eurasia (40°–60°N, 60°–120°E) after detrending, defined as the $WACE_T$ index (the former minus the latter)[5,6]. The positive $WACE_T$ represents the WACE phase, while the negative value represents the CAWE phase. As illustrated by the daily $WACE_T$ index in the winters of 1979/80–2023/24, the $WACE_T$ reversal from early to late winter occurred in 16 winters (see Methods). Among these, 8 winters experienced a reversal from WACE to CAWE, and 8 winters underwent a reversal from CAWE to WACE. Most of the reversal points are around January 10th, manifesting as the opposite $WACE_T$ between periods December 1st to January 10th (Dec1Jan10, defined as early winter) and January 11th to February 28th (Jan11Feb28, defined as late winter) (Supplementary Fig. 1). The SAT anomalies in the Arctic and Eurasian centers both show significant cold/warm transition within a single winter and remain consistent and persistent in each half-winter.

In the composite of these $WACE_T$ reversal years, a significant feature of stratospheric anomalies is the transition of the SPV morphology between contraction and stretching over North America-North Atlantic (Fig. 1a, b). Specifically, when the $WACE_T$ reverses from the CAWE phase in early winter to

the WACE phase in late winter, the SPV undergoes a variation from contraction to a stretched shape over North America. The transition time of the SPV morphology is earlier than the $WACE_T$ reversal, mainly manifested as an evident transition between November 1st–December 15th (Nov1Dec15) and December 16th–February 10th (Dec16Feb10). During Nov1Dec15, the stratospheric anomalies show a zonal asymmetry, with negative potential vorticity (PV) anomalies over North America-North Atlantic and positive anomalies over Eurasia on the 530K isentropic surface (Fig. 1a). However, the PV anomalies transition to a uniform positive pattern in Dec16Feb10, presenting an enhanced SPV, with its center more biased towards North America-North Atlantic (Fig. 1b). The SPV changes in these two periods do not exhibit a completely out-of-phase variation, so the zonal mean stratospheric anomalies cannot capture the evident features well (Supplementary Fig. 2). In both periods, the contraction and stretching of the SPV edge relative to the climate state are most significant over North America-North Atlantic, and the local stratospheric anomalies show significant phase reversal. Therefore, we focus on the linkages between the SPV morphology transition over North America-North Atlantic and the $WACE_T$ phase reversal.

The morphology and shifting of SPV are represented by the area-weighted mean of potential vorticity on the 530K (approximately 44 hPa) over North America-North Atlantic (0–120°W, 60–75°N)[31], defined as the NANA-SPV_{IPV} index. The positive NANA-SPV_{IPV} indicates that the SPV shifts and stretches toward North America-North Atlantic, while a negative NANA-SPV_{IPV} indicates that the SPV moves away from and contracts over North America-North Atlantic (Supplementary Fig. 3). When the SAT pattern changes from CAWE to WACE, the composited NANA-SPV_{IPV} is persistently negative in Nov1Dec15, then turns to positive in mid-December and maintains until February (Fig. 1c). The SPV edge determined by 58PVU on the 530K isentropic surface[32] also clearly reflects the SPV area over North America-North Atlantic transits from contraction to expansion (Supplementary Fig. 4). That is to say, a contracted SPV over North America-North Atlantic in Nov1Dec15 tends to be followed by a CAWE phase in early winter, and a stretched SPV towards North America-North Atlantic in Dec16Feb10 tends to be followed by a WACE phase in late winter. Conversely, the SPV morphology transition from stretching to contracting corresponds to a precursor to the reversal from WACE to CAWE. Both NANA-SPV_{IPV} and $WACE_T$ experience significant phase reversal, and the reversal time of NANA-SPV_{IPV} is approximately 25 days prior to that of $WACE_T$ (Fig. 1c).

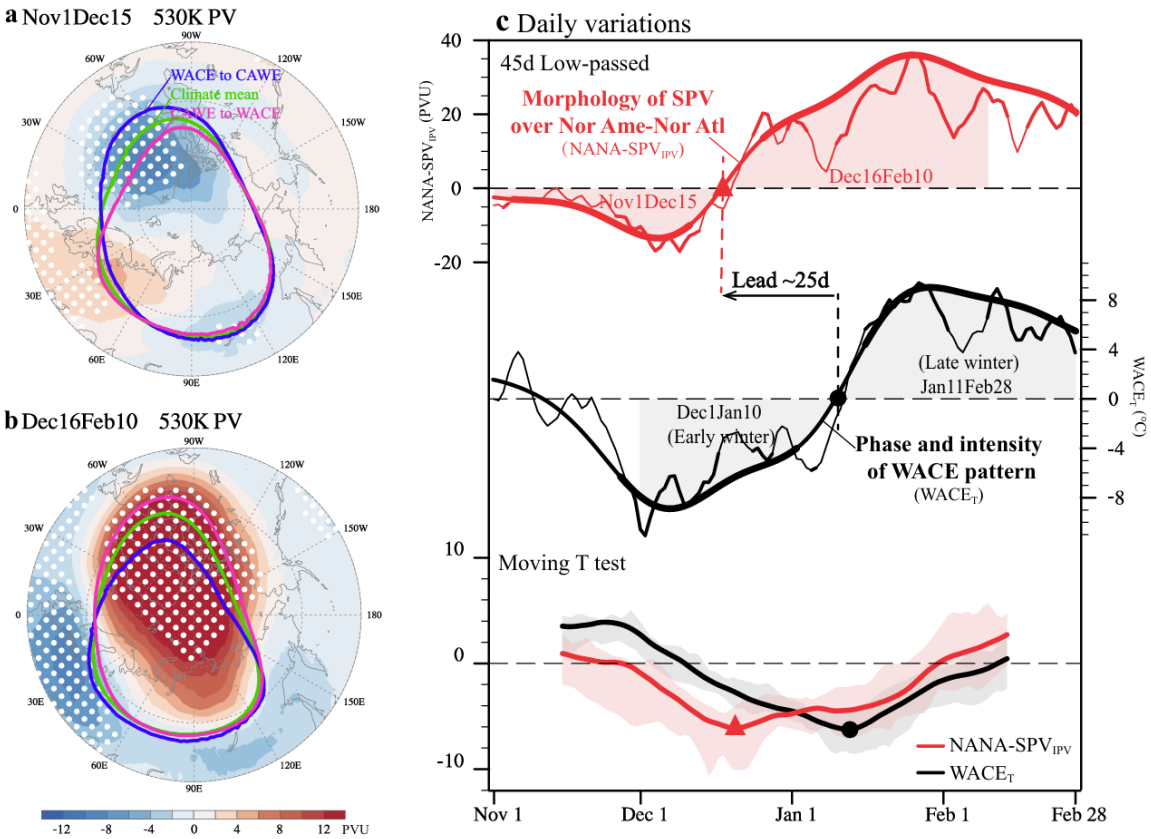

Fig. 1. Linkages between the precursory stratospheric polar vortex and the reversal of "warm Arctic-cold Eurasia". Composites of the potential vorticity on the 530K isentropic surface in (a) November 1st to December 15th and (b) December 16th to February 10th in the "warm Arctic-cold Eurasia" (WACE) pattern reversal years during 1979/80 to 2023/24 (cold Arctic-warm Eurasia (CAWE) to WACE years minus WACE to CAWE years). The green, pink and blue lines represent the composited polar vortex edge in climate mean, CAWE to CAWE years and WACE to CAWE years, respectively. The edge of stratospheric polar vortex is determined by 58PVU on the 530K isentropic. The white dots indicate that the results are significant above the 95% confidence level. (c) The upper part: Daily variations of the stratospheric polar vortex morphology over North America-North Atlantic (NANA-SPV$_{IPV}$; red solid line) and the WACE pattern (WACE$_T$; black solid line) composited in the WACE$_T$ reversal years (CAWE to WACE years minus WACE to CAWE years), and the composited variations after 45-day low-pass filtering are represented by the thick lines. The thicker lines indicate that the results are significant above the 95% confidence level. The red shadings represent the Nov1Dec15 and Dec16Feb10 periods associated with NANA-SPV$_{IPV}$ transitions, and the gray shadings represent the early and late winter associated with WACE$_T$ reversal. The lower part: 45-day moving t-test of the NANA-SPV$_{IPV}$ and WACE$_T$ during November to February in each WACE$_T$ reversal years (shading) and their means (lines), and the most significant point are represented by the markers. The linear trend is removed.

The NANA-SPV$_{IPV}$ and WACE$_T$ processed with a 45-day low-pass filtering can focus more on the phase changes (Fig. 1c). The filtered variations highlight the pronounced transition of the SPV morphology over North America-North Atlantic at mid-December, and more clearly reflect the lead-lag relationship between the NANA-SPV$_{IPV}$ transition and the WACE$_T$ reversal. The moving t-test of NANA-SPV$_{IPV}$ and WACE$_T$ variations can detect the mean-value shift in subsequences (see methods), which also confirms their phase reversal and corresponding time points in the WACE$_T$ reversal years (Fig. 1c).

Further analysis on information flow (see methods) shows that the PV anomalies at 530K over North America-North Atlantic exceed the 95% confidence level for causality (Supplementary Fig. 5), indicating that the NANA-SPV_{IPV} transition plays a pivotal role in modulating the $WACE_T$ reversal. During the longer period from 1950/51 to 2023/24 (25 $WACE_T$ reversal years), the lead-lag linkages between the NANA-SPV_{IPV} transition and the $WACE_T$ reversal still exist (Supplementary Fig. 6). Thus, the SPV morphology transition over North America-North Atlantic is assumed to be one of the important drivers for the phase reversal between WACE and CAWE.

The NANA-SPV_{IPV} can effectively capture the variations in SPV morphology and shift over North America-North Atlantic (Supplementary Fig. 3). Based on the analysis of the daily variation of NANA-SPV_{IPV}, the years when the SPV morphology over North America-North Atlantic undergoes a transition are identified. During 1979/80–2023/24, the significant phase transition of NANA-SPV_{IPV} is observed in 18 years (see Methods), including two types: the SPV morphology transition over North America-North Atlantic from contraction to stretching (9 years) and from stretching to contraction (9 years) (Supplementary Fig. 7). The transition time of NANA-SPV_{IPV} is predominantly concentrated around December 15th. This reversal is characterized by stable yet opposite NANA-SPV_{IPV} anomalies between Nov1Dec15 and Dec16Feb10, and the anomalies in Dec16Feb10 are stronger than that in Nov1Dec15. Additionally, to assess whether the phenomenon of NANA-SPV_{IPV} phase transition is sensitive to the selection of the NANA-SPV_{IPV} reversal timing, we perturbed the division dates by a few days around December 15th and found the results to be consistent. In 12 of the 18 years with NANA-SPV_{IPV} transition, the $WACE_T$ reverses from early to late winter (Supplementary Fig. 8), covering up to 75% of the winters with WACE reversal.

The stratospheric anomalies associated with $WACE_T$ reversal are deep and barotropic on the vertical structure, especially over the North America-North Atlantic (Supplementary Fig. 9a). Both during Nov1Dec15 and Dec16Feb10, the opposite geopotential height anomalies over North America-North Atlantic can extend from the stratosphere down to the near surface. This phenomenon can also be observed in the westerly jet surrounding SPV over North America-North Atlantic. The anomalies of geopotential height and zonal wind in Dec16Feb10 are stronger and last longer than those in Nov1Dec15. Correspondingly, the $WACE_{T'}$ in Jan11Feb28, lagging NANA-SPV_{IPV} by about 25 days, is more

prominent and persistent (Fig. 1c), indicating an enhanced impact of NANA-SPV_{IPV} in Dec16Feb10. The stratospheric anomalies of geopotential height and the zonal wind over Eurasia are opposite with those over North America-North Atlantic in Nov1Dec15 (Supplementary Fig. 2). These anomalies can also extend from the middle stratosphere to the near-surface, indicating the barotropy of the zonal asymmetric pattern. During the Dec16Feb10 period, the center of the stratospheric signal is more concentrated over North America-North Atlantic, while it is relatively weak over Eurasia and fails to effectively propagate downward (Supplementary Fig. 9b). Thus, an important stratospheric precursor associated with the $WACE_T$ reversal is the SPV morphology transition over North America-North Atlantic. This raises a question of how the SPV morphology transition over North America-North Atlantic drives the WACE pattern to reverse.

Cross-continental physical processes modulated by the SPV

The SPV variations correlate closely with the tropospheric atmosphere through stratosphere-troposphere coupling processes, thereby affecting the occurrence of extreme weather and climate[20]. When a negative NANA-SPV_{IPV} occurs in Nov1Dec15, the SPV morphology is contracted over North America-North Atlantic. The geopotential height anomalies at 50 hPa form a zonal asymmetrical pattern, with positive anomalies over North America-North Atlantic and negative anomalies over western Eurasia, which are consistent with the stratospheric anomalies when $WACE_T$ reverses (Fig. 2a). We use the Plumb wave activity fluxes averaged over 60°–70°N as a function of longitude and pressure to investigate the role of vertical wave coupling[21]. The Plumb fluxes in the lower stratosphere over North America-North Atlantic are predominantly upward (Supplementary Fig. 10a), contributing to the enhancement and persistence of the anomalous stratospheric high pressure over North America-North Atlantic. The upward and eastward propagating Plumb waves form anomalous downward wave activity flux over Western Europe, accompanied by the negative geopotential height anomalies that propagate from the stratosphere to the troposphere (Fig. 3a).

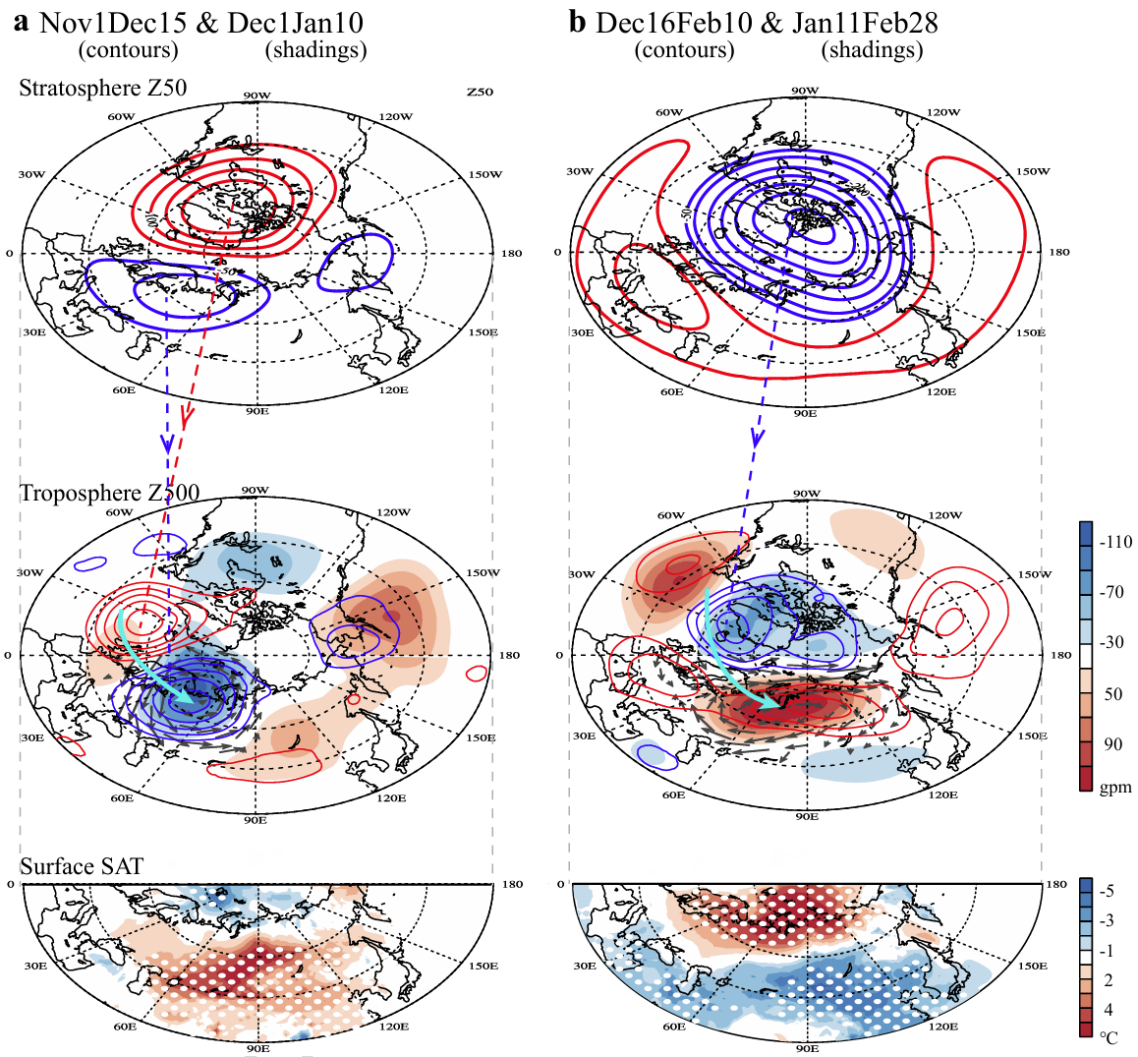

Fig. 2. Responses of the atmospheric circulations and surface air temperature to the stratospheric polar vortex morphology transition over North America-North Atlantic. (a) Composites of the geopotential height at 50 hPa in Nov1Dec15 (the top panel), the geopotential height at 500 hPa in Nov1Dec15 (contours) and in Dec1Jan10 (shadings), the wind at 850 hPa in Dec1Jan10 (arrow, the middle panel), and the surface air temperature (SAT) in Dec1Jan10 (the bottom panel) according to the transition of stratospheric polar vortex morphology over North America-North Atlantic ($NANA\text{-}SPV_{IPV}$) during 1979/80 to 2023/24 (negative to positive $NANA\text{-}SPV_{IPV}$ years minus positive to negative $NANA\text{-}SPV_{IPV}$ years). (b) Composites of the geopotential height at 50 hPa in Dec16Feb10 (the top panel), the geopotential height at 500 hPa in Dec16Feb10 (contours) and in Jan11Feb28 (shadings), the wind at 850 hPa in Jan11Feb28 (arrow, the middle panel), and the SAT in Jan11Feb28 (the bottom panel) according to $NANA\text{-}SPV_{IPV}$ transition during 1979/80 to 2023/24. The cyan arrows represent the propagation of the Plumb wave at the 500 hPa in Nov1Dec15 and Dec16Feb10. The contours and shadings in the top and middle panels and the white dots in the bottom panels indicate that the results are significant above the 95% confidence level.

In the troposphere, the positive geopotential height anomaly over North America-North Atlantic and the negative anomaly over Western Europe form a Rossby wave propagating eastward (Supplementary Fig. 11a). This is conducive to a notable positive PV anomaly at 315K and anomalously increased static

stability in the Ural Mountains region (Supplementary Fig. 12), thereby suppressing the Ural blocking activities[33] (Fig. 2a). The weakened Ural high can last until mid-January and forms the sustained southerly winds in the mid-high latitudes of Eurasia (Supplementary Fig. 11c), which hinder the southward transport of cold air and gather the cold air in the Barents-Kara Seas, thus resulting in a significant CAWE anomaly during early winter (Fig. 2a, 3c).

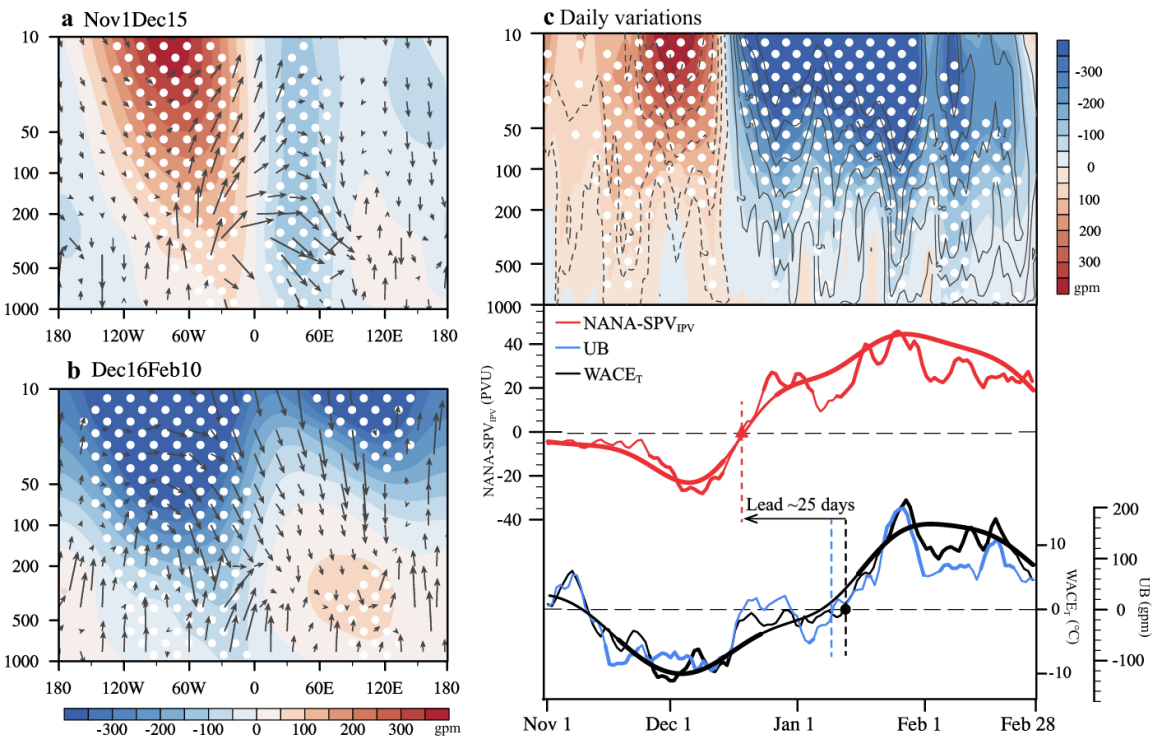

Fig. 3. Physical mechanisms of the stratospheric polar vortex morphology transition over North America-North Atlantic impacting the reversal of "warm Arctic-cold Eurasia". Composites of the anomalous geopotential height (shading) and the vertical and zonal components of anomalous Plumb wave activity flux (vector) averaged over 60°–70°N as a function of longitude and pressure in (a) Nov1Dec15 and (b) Dec16Feb10 according to the transition of stratospheric polar vortex morphology over North America-North Atlantic (NANA-SPV$_{IPV}$) during 1979/80 to 2023/24 (negative to positive NANA-SPV$_{IPV}$ years minus positive to negative NANA-SPV$_{IPV}$ years). The magnitude of the Plumb flux is scaled by $(1000/p)^{1/2}$. (c) Composites of the daily variations of the pressure-temporal geopotential height (shadings) and zonal wind (contours) along 0–120°W, 60–70°N, and the daily variations of NANA-SPV$_{IPV}$, Ural blocking (UB) and "warm Arctic-cold Eurasia" pattern (WACE$_T$) index according to NANA-SPV$_{IPV}$ transition during 1979/80 to 2023/24 (negative to positive NANA-SPV$_{IPV}$ years minus positive to negative NANA-SPV$_{IPV}$ years). The composited variations after 45-day low-pass filtering are represented by the smooth lines. The thicker lines indicate that the results are significant above the 95% confidence level. The white dots indicate that the results are significant above the 95% confidence level.

When the NANA-SPV$_{IPV}$ transits from negative to positive, the SPV appears to be stretched towards North America-North Atlantic in Dec16Feb10. The entire Arctic region is covered by an enhanced SPV, with the center of anomalies biased towards North America-North Atlantic (Fig. 2b). Over North America-

North Atlantic, anomalous downward propagation of the Plumb vertical flux is observed (Fig. 3b, Supplementary Fig. 10b). The negative geopotential height anomalies and intensified zonal winds propagate strongly and persistently from the stratosphere to the troposphere (Fig. 3c), contributing to the formation of a positive NAO phase (Fig. 2b). The Rossby wave train triggered by the stratospheric atmosphere anomaly is generated in the mid-latitudes of the North Atlantic (Supplementary Fig. 11b, d), serving as a wave source[34]. The wave activity flux in the troposphere propagates eastward and causes the abnormal high pressure over Western Europe and the mid-high latitudes of Eurasia. The persistence of this Rossby wave makes the Ural High enhanced and sustained in late winter (Fig. 2b). In addition, the eddy vorticity forcing forms a positive synoptic eddy feedback (see Methods), and further enhances the tropospheric response[35]. Under the influence of enhanced SPV, the eddy vorticity forcing in the North Atlantic is conducive to the maintenance of a positive NAO phase. The divergent eddy vorticity fluxes over Western Europe and the Ural region generate an anticyclonic forcing (Supplementary Fig. 13), which strengthens and maintains the Ural blocking in late winter. Driven by the intensified Ural high, a pronounced WACE phase occurs in late winter that is opposite to that in early winter (Fig. 2b, 3c).

In the real case observed in 1983/84, a typical NANA-SPV_{IPV} transition from negative to positive occurred, leading to a $WACE_T$ reversal with a lag of about 25 days (Supplementary Fig. 14). An abnormal positive pressure center at 50 hPa was located over North America-North Atlantic in Nov1Dec15 of 1983/84, but there was a negative pressure center over Eurasia, representing a contraction of the SPV area over North America-North Atlantic (Supplementary Fig. 14a). While in Dec16Feb10, the SPV expanded sharply towards North America-North Atlantic, with a remarkable negative geopotential height anomaly at 50 hPa (Supplementary Fig. 14b). Affected by the downward influence of the stratospheric anomalies and the propagation of tropospheric Rossby waves (Supplementary Fig. 15), the Ural high intensity underwent a significant variation from weakened in early winter to enhanced in late winter, thus causing a phase reversal from CAWE to WACE (Supplementary Fig. 14c). The stratospheric anomaly in Dec16Feb10 was stronger than that in the other sub-period, thereby causing a more pronounced response of Ural high and $WACE_T$ in late winter. East Asia was affected by the significant WACE phase and experienced a severe cold wave in January and February of 1984[36].

The NANA-SPV_{IPV} transition is approximately 25 days ahead of the $WACE_T$ phase reversal (Fig.

1c), which may be related to the time required for the downward transmission of stratospheric signal and the excitation and propagation of Rossby waves[37]. This time interval is coordinated with a maximum suppression of Ural blocking observed around day 24 following the SPV weakening[33]. The downward influences of the SPV morphology transition indicate the modulations from the stratospheric variability on the phase variations of SAT pattern in the Arctic-Eurasian region, deepening the understanding of the widely concerned cold-warm transition events from a fresh perspective of stratosphere-troposphere coupling[38].

Simulations of the key processes and linkages

To further determine the robustness of the linkages between the variation of SPV morphology over North America-North Atlantic and the WACE$_T$ phase reversal, and verify the proposed physical processes, we performed the analysis using historical simulations of the Coupled Model Intercomparison Project Phase 6 (CMIP6) from 1950–2014 and the Community Earth System Model large ensemble (CESM-LM) experiments from 1920–2005 (see methods). The simulations of 21 CMIP6 models and 39 CESM-LE members, which have daily data and are available for download, are used for analysis. Since the PV variable is not directly available in simulations, we use the 50 hPa geopotential height to identify the years with the SPV morphology transition[39]. The conclusions obtained from the reanalysis using the PV at 530K and the geopotential height at 50hPa are consistent (see Methods for detailed explanations).

Specifically, the case is selected as the SPV morphology transition over North America-North Atlantic from contraction to stretching based on these two conditions: (1) the area-weighted mean of geopotential height anomalies at 50 hPa over North America-North Atlantic transits from positive in Nov1Dec15 to negative in Dec16Feb10; (2) the geopotential height anomalies in Nov1Dec15 present a zonal asymmetry over North America-North Atlantic and Eurasia, which is defined as the simulated "Con-to-Stre NANA-SPV" case (Supplementary Fig. 16a, b). Conversely, the case is defined as the simulated "Stre-to-Con NANA-SPV" to represent the SPV morphology transition over North America-North Atlantic from stretching to contraction (Supplementary Fig. 16c, d). In the CMIP6 and CESM-LE simulations, the SPV morphology transitions over North America-North Atlantic between Nov1Dec15 and Dec16Feb10 occur in 27% and 28% of the years (Fig. 4a), respectively, which are lower than the

observed frequency of NANA-SPV$_{IPV}$ transition (40%).

The WACE$_T$ reversal represents a significant WACE$_T$ difference between early and late winter (the latter minus the former, defined as Diff-WACE$_T$). We first verify whether the SPV morphology transition over North America-North Atlantic can lead to the corresponding Diff-WACE$_T$ through the model simulations. In the 200 cases of simulated Con-to-Stre NANA-SPV, the mean Diff-WACE$_T$ is positive (Fig. 4a), and the distribution of SAT difference over Arctic-Eurasia exhibits a notable WACE anomaly (Supplementary Fig. 17a). Among these 200 cases, 72% show a positive Diff-WACE$_T$, indicating that the transition of SPV morphology over North America-North Atlantic from contraction to stretching is conducive to the reversal towards the WACE phase. In the 176 cases of simulated Stre-to-Con NANA-SPV, the mean SAT difference in all such years shows a significant CAWE anomaly (Supplementary Fig. 17b). The negative Diff-WACE$_T$ can be captured in 71% of these years, indicating a tendency and a higher probability to reverse to CAWE phase (Fig. 4a). The two transition types based on CESM-LE simulations, which have a larger sample size, also strongly verify that the SPV morphology transition over North America-North Atlantic facilitates the reversal between WACE and CAWE phase from early to late winter (Supplementary Fig. 17c, d). However, the responses of Diff-WACE$_T$ associated with the SPV morphology transitions over North America-North Atlantic simulated by CMIP6 and CESM-LE are both weaker than the reanalysis results (Fig. 4a).

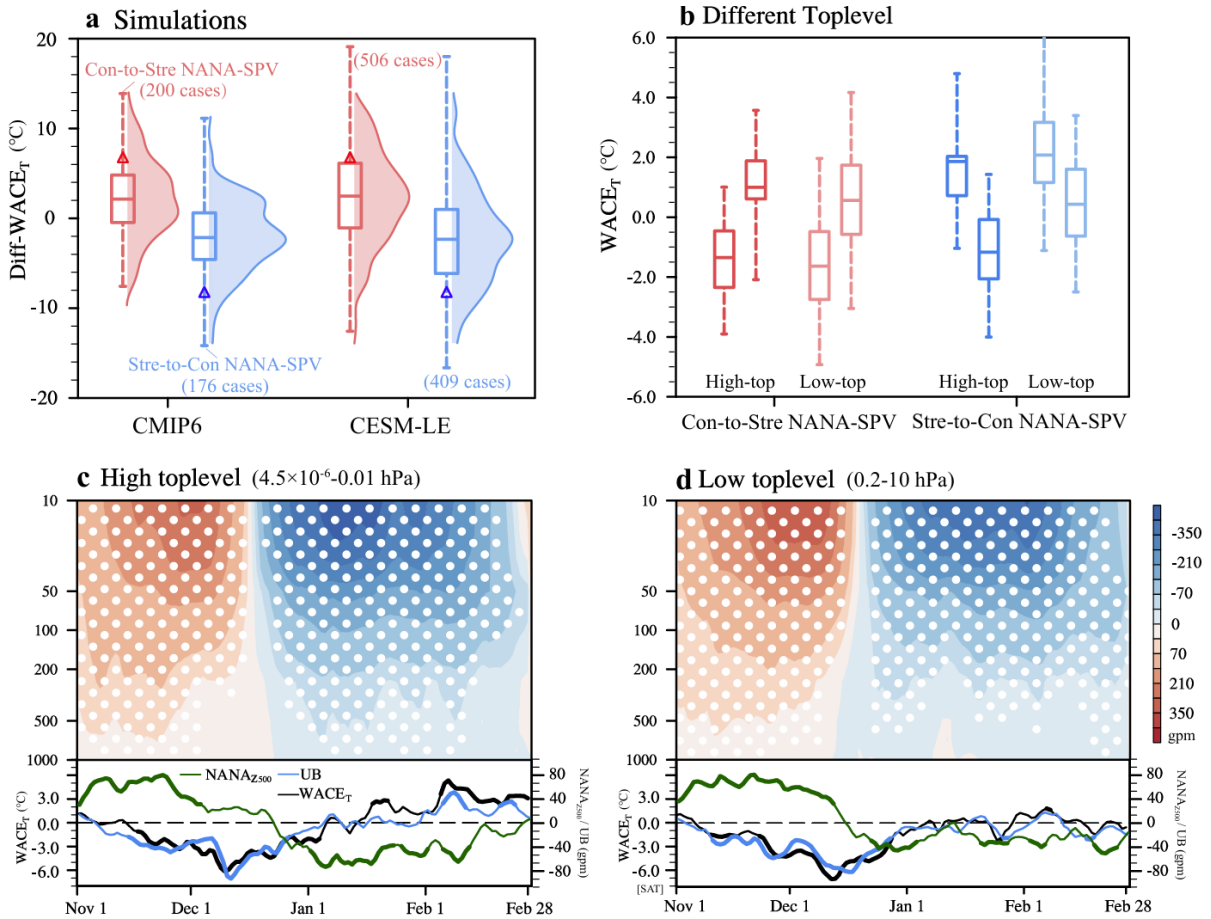

Fig. 4. Verifications of the physical linkages in simulations. (a) Multi-member mean and the probability distribution of the simulated difference of "warm Arctic-cold Eurasia" pattern between early and late winter (Diff-WACE$_T$) in the simulated transition of stratospheric polar vortex morphology over North America-North Atlantic from contraction to stretching (Con-to-Stre NANA-SPV) years (red) and from stretching to contraction (Stre-to-Con NANA-SPV) years (blue) based on CMIP6 simulations and CESM-LE simulations. The center line, box limits and whiskers of the box-plots elements are defined as mean, upper and lower quartiles, maximum and minimum, respectively. The hollow triangles represent the reanalysis results. (b) The simulated "warm Arctic-cold Eurasia" pattern (WACE$_T$) in early and late winter in the simulated Con-to-Stre NANA-SPV years (red) and Stre-to-Con NANA-SPV years (blue) based on the High-top and Low-top CMIP6 models. The center line, box limits and whiskers of the box-plots elements are defined as mean, upper and lower quartiles, maximum and minimum, respectively. (c, d) Composites of the pressure-temporal geopotential height along 0–120°W, 60–75°N, and the daily variation of the geopotential height anomalies at 500 hPa over the North America-North Atlantic (NANA$_{Z500}$), Ural blocking (UB) and WACE$_T$ according to the simulated stratospheric polar vortex morphology transition (Con-to-Stre NANA-SPV years minus Stre-to-Con NANA-SPV years) that selected from the High-top and Low-top CMIP6 models. The white dots and the thicker lines indicate that the results are significant above the 95% confidence level.

However, there is a large spread of simulated Diff-WACE$_T$ in Con-to-Stre NANA-SPV and Stre-to-Con NANA-SPV years in different CMIP6 models, and not all models can capture the physical linkages between the two well. The model top height is revealed to be one of the key factors restricting the model simulation ability of the stratosphere-troposphere interactions[40]. We categorize the models into high-top

and low-top groups based on whether their model top level reaches 0.1 hPa, thereby comparing their simulation capabilities for the SPV morphology transition and its influence on WACE phase reversal. The high-top and low-top model groups consist of 9 and 12 models, respectively, with the ranges of top level being 4.5×10^{-6}–0.1 hPa and 0.2–10 hPa, respectively (Supplementary Table 1).

Both the high-top and low-top models can simulate the variations of the geopotential height anomalies at 50 hPa during Nov1Dec15 and Dec16Feb10 associated with the SPV morphology transition over North America-North Atlantic (Fig. 4c, d). In the years when the SPV morphology undergoes transition, the accuracy rates for the sign of the simulated Diff-WACE$_T$ in the high-top and low-top models are 76% and 69%. The accuracy rate refers to the proportion of cases in which a positive Diff-WACE$_T$ is simulated in Con-to-Stre NANA-SPV cases and a negative Diff-WACE$_T$ is simulated in Stre-to-Con NANA-SPV cases. A higher accuracy rate of high-top models indicates that they have a better simulation ability for the linkage between SPV morphology transitions and WACE$_T$ phase reversal. Specifically, both the high-top and low-top models can simulate the WACE$_T$ response in early winter, but significant differences exist in simulations of the WACE$_T$ in late winter (Fig. 4b). The high-top models can more accurately reproduce the WACE$_T$ phase reversal, and the opposite WACE$_T$ between early and late winter can be clearly distinguished. Especially for the type where the SPV changes from stretching to contraction, the high-top models effectively simulate the SAT pattern reversing from WACE to CAWE, while the low-top models cannot capture the phase reversal in late winter.

The discrepancy in simulating the WACE$_T$ response between the high-top and low-top models may stem from the differences in their simulation of the stratospheric anomaly intensity in Dec16Feb10. Both the high-top and low-top models are capable of simulating the weakened Ural high, which is associated with the downward influence of the stratospheric zonal asymmetry (Supplementary Fig. 18, 19). The positive geopotential height anomalies over North America-North Atlantic and negative anomalies over western Eurasia at 50 hPa in Nov1Dec15 lead to the CAWE phase in early winter (Fig. 4c, d). However, when stratospheric anomalies undergo a phase reversal, the high-top models simulate a stronger intensity of the geopotential height anomaly at 50 hPa over North America-North Atlantic in Dec16Feb10 compared to that simulated by low-top models (Fig. 4c), with an approximate enhancement of 18%. The high-top models can better capture the downward propagation intensity of stratospheric anomalies. The

response of the geopotential height anomalies over the North America-North Atlantic region (defined as $NANA_{Z500}$) is more significant (Supplementary Fig. 18d), which is more conducive to the formation and propagation of Rossby waves in the troposphere, ultimately enhancing the Ural High and promoting a reversal toward the WACE phase in late winter (Fig. 4c, Supplementary Fig. 18f).

In contrast, the low-top models simulate weaker stratospheric signals and their corresponding downward propagation over North America-North Atlantic in Dec16Feb10, and the response in the troposphere extends to the western European coast (Fig. 4d, Supplementary Fig. 19d), which is unfavorable for the establishment of the Ural high in late winter and the formation of the WACE phase (Supplementary Fig. 19f). The high top-level models, with comprehensive stratospheric representation, well simulate and verify the physical linkages through which the SPV morphology transition modulates the $WACE_T$ reversal between early and late winter through cross-continental process. Models with a higher top level are more conducive to simulating the stratosphere-troposphere coupling and its impacts on near-surface extreme climate, further providing key evidence that model design and construction should be extended to higher levels.

Discussions

In this study, we mainly reveal that the transition of SPV morphology over North America-North Atlantic plays a prominent role in modulating the phase reversal between WACE and CAWE (Fig. 5). The downward influence of stratospheric precursor and the dispersion of Rossby wave establish a bridge for SPV variations over North America-North Atlantic to impact the climate variability in Arctic-Eurasia. The high-top CMIP6 models effectively simulate these physical linkages and mechanisms, especially well reproducing the Ural high reversal in late winter compared to the low-top models. However, the verification using the CMIP6 and CESM-LE experiments is a qualitative simulation, and sensitivity experiments are needed to directly control the intensity and distribution of stratospheric anomalies. Such experiments may further clarify why stratospheric changes over North America-North Atlantic exhibit a stronger correlation with $WACE_T$ reversal. The triggering mechanism for such rapid NANA-SPV_{IPV} phase reversal may be related to the changes in intensity of upward planetary waves entering the stratosphere and the eddy heat transport to the pole[41]. These changes can be traced back to tropospheric perturbations such as blockings and the westerly jet[17,42], as well as to the climate forcing factors such as the reduction

of Arctic sea ice[43], the increase of Siberian snow cover[44] and the El Niño-Southern Oscillation[45].

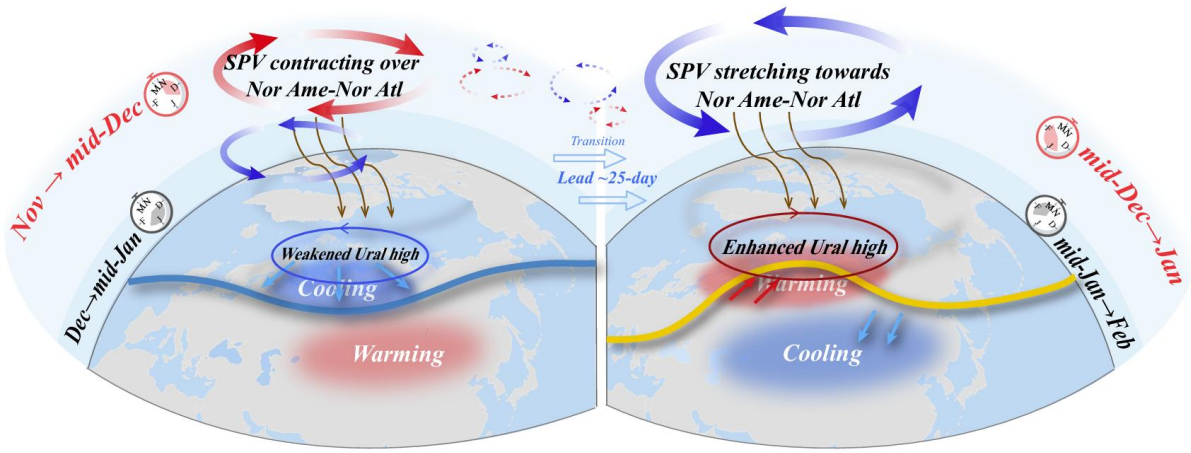

Fig. 5. The timeline and physical process of the stratospheric polar vortex morphology transition over North America-North Atlantic modulating the phase reversal of "warm Arctic-cold Eurasia". The contracted stratospheric polar vortex (SPV) over North America-North Atlantic with zonal asymmetric anomalies in Nov1Dec15 causes the suppressed Ural high in early winter through the vertical wave coupling and transmission of the Rossby wave, leading to the cold Arctic-warm Eurasia phase. While in Dec16Feb10, the SPV stretches toward North America-North Atlantic and enhances across the Arctic, causing the sustained Ural blocking in late winter through downward-propagation and synoptic eddy feedback, resulting in the warm Arctic-cold Eurasia phase opposite to that in early winter. The red and blue arrows indicate abnormal anticyclones and cyclones. The dotted arrow indicates the evolution of stratospheric anomalies. The blue and yellow thick lines represent the geopotential height at 500 hPa. The clock indicates the period from November to March, and the red and grey shadows in the clock indicate the duration of the two stages of the SPV morphology and "warm Arctic-cold Eurasia" pattern. The SPV morphology transition leads the phase reversal of "warm Arctic-cold Eurasia" pattern by about 25 days.

Previous studies revealed that the synergistic effect of the preceding tropical-subtropical SST anomalies in the North Atlantic and the Indian Ocean can also cause the WACE$_T$ to reverse[6]. Based on a relatively simple and linear method of constructing a regression model (see Methods), the SPV variability and tropical-subtropical SST signals together explain 59% of the WACE$_T$ reversal intensity. These two factors are independent of each other, with the correlation coefficient at 0.26 (insignificant). The SPV and tropical-subtropical SST anomalies contribute 39% and 20%, respectively, indicating an effective driving force from the stratosphere. The revelation of stratospheric precursors is particularly important for the explanations of Arctic-Eurasia climate variability in late winter, compensating for the insufficiency of trigger factors and predictable sources within the troposphere[46]. The significant simulation differences between the high and low top-level models highlight the complexities of the potential mechanisms of stratosphere-troposphere coupling. Accurately simulating the interactions between the stratosphere and troposphere remains a considerable challenge[47]. The high-top models have high skill in simulating the

downward influence of stratospheric precursor and its role in climate variability in the Arctic-Eurasia, which may offer an effective solution and future development direction for improving the simulation of the stratosphere-troposphere interaction.

The pronounced variations in Arctic-Eurasia climate anomalies between early and late winter pose great challenges and obstacles for seasonal prediction[48]. The significant contribution of SPV variations to the WACE pattern provides a potential prediction implication for the climate variability in the Arctic and mid-high latitudes of Eurasia[49]. To truly predict the subseasonal to seasonal variations of the WACE pattern, it is necessary to comprehensively consider multiple signals, including the stratosphere, Arctic change and tropical SST. More importantly, the Arctic-Eurasia climate variability serves as drivers and predictable sources for extreme climate and in environmental disasters in the mid-low latitudes[50,51]. The persistent large-amplitude atmospheric circulations accompanied by the WACE pattern exacerbate the extremity of the climate anomalies[9,50]. The impacts of the stratospheric atmosphere on the Arctic-Eurasia climate variability can also have a chain reaction on the climate extremes in the mid-low latitudes. Explorations of changes in the stratosphere and their impacts enhance the understanding of the crucial role of stratosphere-troposphere coupling in extreme climate.

Methods

Data treatment and statistical methods

In this study, we use the ERA5 reanalysis data for analysis[52]. The linear trend and its long-term (1979/80–2023/24) mean of all the daily data are removed, which indicates that the seasonal cycle is also removed. The method of detrending is to first calculate the slope and intercept of the least squares linear trend line of the original variables during 1979/80–2023/24, and obtain the linear trend term of year(i) as slope×year(i)+intercept, and then remove the linear trend term from the original variables to obtain the detrended results.

In this study, the statistical methods such as correlation coefficient, composite analysis, trend analysis, significance tests, and moving t-test are used[53]. The type of correlation coefficient used in this study is Pearson correlation, which measures the linear relationship between two random variables. The linear trends during the different sub-periods are calculated by the least squares method. A two-sided student's t-

test is used to test the statistical significance of the composite analysis. The significance of the correlation and the slope rates of the linear trends during the different sub-periods can be tested by using the student's t-test. The 95% confidence level is denoted by $p < 0.05$. The moving t-test can examine whether the difference between the means of two sample groups is statistically significant, in order to detect the abrupt change point. In this study, a sample length of 45 days is adopted, which effectively captures the phase variation and shift on the subseasonal scale.

The Liang–Kleeman (L-K) information flow analysis is applied to verify the causal relationship between the NANA-SPV_{IPV} transition and the $WACE_T$ reversal. The causality is measured by the time rate of information flowing from one series to the other. In this study, a causal analysis is conducted on the 30-day time series of the NANA-SPV_{IPV} phase transition process (December 1st to December 30th) and the $WACE_T$ reversal process (December 26th to January 25th). These 30 days represent the 15 days before and 15 days after the reversal point of NANA-SPV_{IPV} and $WACE_T$. According to theory, the maximum likelihood estimation form of the information flow from time series X2 to time series X1 under the assumption of the linear model is as follows:

(1) $$T_{2\to1} = \frac{C_{11}C_{12}C_{2,d1} - C_{12}^2 C_{1,d1}}{C_{11}^2 C_{22} - C_{11}C_{12}^2}$$

where C_{ij} is the sample covariance between X_i and X_j, and $C_{i,dj}$ is the covariance between X_i and $\{(X_{j,n+1} - X_{j,n})/\partial t\}$, with ∂t representing the time interval. According to the L-K theory, causation implies correlation. However, the converse is that correlation does not imply causation. When $|T_{2\to1}| > 0$, X_2 is a cause of X_1; and when $|T_{2\to1}| = 0$, X_2 is not a cause of X_1[54].

Definitions of the $WACE_T$ phase reversal and NANA-SPV_{IPV} transition

The $WACE_T$ phase reversal needs to satisfy two conditions: (1) the $WACE_T$ in early winter and late winter is reversed after the removal of the trend and climate mean of 1979/80–2023/24; and (2) the sum of the standard deviation in early winter and late winter after the standardization of daily $WACE_T$ in December 1st to February 28th is < 1.8. The second condition picks out the persistent WACE or CAWE stage in half-winter. The threshold of 1.8 is selected based on a summary of year-by-year analyses of daily $WACE_T$ index that met the first condition, excluding years that primarily exhibited fluctuating variations. Minor adjustments to this threshold do not affect the feature of $WACE_T$ phase reversal. In this study, the

early winter and late winter are divided by January 10th, meaning early winter spans from December 1st to January 10th, and late winter spans from January 11th to February 28th. To verify the reliability of the $WACE_T$ reversal years selected by this method, we perturbed the division dates for a few days before and after January 10th and found the results consistent.

Using the above similar methods to define the NANA-SPV_{IPV} transition, two conditions also need to be met: (1) the NANA-SPV_{IPV} in periods Nov1Dec15 and Dec16Feb10 is reversed after the removal of the trend and climate mean of 1979/80–2023/24; and (2) the sum of the standard deviation in periods Nov1Dec15 and Dec16Feb10 after the standardization of daily NANA-SPV_{IPV} in November 1st to February 10th is < 1.6. Similarly, the threshold of 1.6 is selected based on a summary of year-by-year analyses of daily NANA-SPV_{IPV} index that met the first condition, excluding years that primarily exhibited fluctuating variations. Minor adjustments to this threshold do not affect the conclusions of this study. In addition, when perturbing the division date (December 15th), the selected NANA-SPV_{IPV} transition years remained consistent.

By applying the empirical orthogonal function (EOF) analysis over the latitude-time (day) domain to daily geopotential height anomaly at 50 hPa zonally averaged from 0° to 120°W[55], the spatiotemporal evolution of the NANA-SPV_{IPV} transition is further explained. The combined manifestation of EOF1 and EOF3 can effectively capture the variation of geopotential height anomaly associated with the NANA-SPV_{IPV} transition (Supplementary Fig. 20). The presentation of the EOF pattern is robust, which has undergone sensitivity tests using the additional period 1950/51–1978/79. The specific manifestation is that the stratospheric anomaly over North America-North Atlantic reverses at around mid-December, and the anomaly is stronger during the Dec16Feb10 period. The sum of these two mode's time series in the NANA-SPV_{IPV} reversal years is generally extreme (Supplementary Fig. 20g), further indicating the importance of studying such events.

Plumb wave activity flux

We used the 3D Plumb wave activity flux to examine zonal, meridional, and vertical wave propagation of quasi-stationary waves[56].

$$(F_\lambda, F_\varphi, F_z) = p\cos\varphi \begin{cases} v'^2 - \frac{1}{fa\cos\varphi}\frac{\partial(v'\Phi')}{\partial\lambda} \\ -u'v' + \frac{1}{fa\cos\varphi}\frac{\partial(u'\Phi')}{\partial\lambda} \\ \frac{f}{\partial\tilde{T}/\partial z + \kappa\tilde{T}/H}\left[v'T' - \frac{1}{fa\cos\varphi}\frac{\partial(T'\Phi')}{\partial\lambda}\right] \end{cases} \quad (2)$$

where λ is longitude, φ is latitude, z is height, and p is pressure. u is the zonal wind, v is the meridional wind, T is temperature, and Φ is geopotential height. f is the Coriolis parameter. a is Earth's radius. κ is the specific gas constant of dry air divided by the specific heat of dry air. $\tilde{T}$ denotes the domain average of temperature. H is the log-pressure scale height. Primes denote the deviations from zonal means.

Eddy vorticity forcing

The stream function tendency induced by eddy-vorticity fluxes, namely eddy-vorticity forcing (EVF), can measure the dynamic synoptic eddy feedback onto the low frequency flow[57]. The EVF can be expressed as

$$\left(\frac{\partial\psi^a}{\partial t}\right)_{se} = -\Delta^{-1}\nabla\cdot[V'\zeta']^a \quad (3)$$

where $V'(u', v')$ and ζ' denote the 2–8-day bandpass filtered zonal wind, meridional wind, and vorticity, respectively. $[\,]^a$ denotes the anomaly during Dec16Feb10 period. $\nabla\cdot(\,)$ and $\Delta^{-1}(\,)$ are the horizontal divergence and the Laplacian inversion operators, respectively. $(\,)_{se}$ indicates the tendency induced by synoptic eddy. The positive (negative) EVF can contribute to a positive (negative) tendency of the stream function, which expresses an anticyclonic (cyclonic) vorticity tendency.

Calculation methods for the contribution of $WACE_T$ reversal intensity

The intensity of the $WACE_T$ reversal is denoted as the $WACE_T$ difference between early and late winter (defined as Diff-$WACE_T$). The NANA-SPV_{IPV} difference between Nov1Dec15 and Dec16Feb10 serves as the intensity of the stratospheric anomalies. The SST anomalies in the tropical Atlantic and Indian oceans had significant primary impacts on the WACE/CAWE pattern in early and late winter, respectively[6]. Their synergistic effect effectively modulates the phase reversal between the WACE and CAWE. Therefore, the sum of the standardized time series of these two SST factors is used to represent the tropical-subtropical SST anomaly signals. After standardizing the time series of tropical-subtropical SST signals and stratospheric signals, a linear regression is performed against Diff-$WACE_T$. The

contribution of stratospheric anomalies to the $WACE_T$ reversal intensity in a given year is calculated by multiplying the regression coefficient of the stratospheric anomalies by their standardized anomaly value in that year[58]. The average across all $WACE_T$ reversal years represents the contribution of stratospheric anomalies. The same method is applied to obtain the contribution of tropical-subtropical SST signals.

CMIP6 and CESM-LE simulations

To verify the strong linkage between NANA-SPV_A transition and $WACE_T$ reversal, the Coupled Model Intercomparison Project Phase 6 (CMIP6)[59] historical simulations and the Community Earth System Model large ensemble (CESM-LE)[60] simulations are used to complement the statistical analyses. Daily surface air temperature and geopotential height on pressure levels from the historical simulations of 21 available CMIP6 models from 1950 to 2014 and from 39 members of the Community Earth System Model from 1920–2005 are employed in this study. Similar to the process of observations, the linear trends during 1950–2014 in the CMIP6 simulations and during 1920–2005 in the CESM-LE simulations are removed to obtain the daily anomaly.

Since the PV variable is not directly available in simulations, we use the 50 hPa geopotential height to identify the years with the SPV morphology transition[39]. In the $WACE_T$ reversal year, both the PV at 530K and the geopotential height at 50 hPa over North America-North Atlantic undergo significant phase reversals (Supplementary Fig. 21). The daily variations of these two indices are basically the same, only with opposite signs. The reversal time points of these two indices are basically consistent. When the NANA-SPV_{IPV} transits, the geopotential height anomaly also shows a phase reversal over North America-North Atlantic between Nov1Dec15 and Dec16Feb10, with a zonal asymmetric pattern in Nov1Dec15 (Supplementary Fig. 2a). Among the 18 years of observed NANA-SPV_{IPV} transition, 17 years exhibit these characteristics. Therefore, using these definitions to identify the cases of SPV morphology transition over North America-North Atlantic in the simulation is relatively reasonable and reliable.

In CMIP6 and CESM-LE simulations, the cases are selected as the SPV morphology transition over North America-North Atlantic from contraction to stretching based on these two conditions: (1) the area-weighted mean of geopotential height anomalies at 50 hPa over North America-North Atlantic transits from positive in Nov1Dec15 to negative in Dec16Feb10; (2) the geopotential height anomalies in

Nov1Dec15 present a zonal asymmetry over North America-North Atlantic and Eurasia. Conversely, the cases represent the SPV morphology transition over North America-North Atlantic from stretching to contraction. In addition, we explore the simulation capabilities of the CMIP6 models with different top height. The models are divided into high-top and low-top groups based on whether the model top level reaches 0.1 hPa. The high-top and low-top model groups consist of 9 and 12 models, respectively, with the ranges of top level being 4.5×10^{-6}–0.1 hPa and 0.2–10 hPa, respectively.

Data availability

Daily meteorological data on surface and pressure levels from ERA5 including surface air temperature, potential vorticity, geopotential height, zonal wind, meridional winds are available at https://cds.climate.copernicus.eu/datasets/reanalysis-era5-single-levels?tab=overview and https://cds.climate.copernicus.eu/datasets/reanalysis-era5-pressure-levels?tab=overview. Daily surface air temperature and geopotential height of CMIP6 historical simulation are available at https://esgf-metagrid.cloud.dkrz.de/search. Daily surface air temperature and geopotential height at 50 hPa of CESM-LE historical simulation are available at https://gdex.ucar.edu/datasets/d651027/dataaccess/#. The data underlying each figure of this study are available in the Zenodo repository https://doi.org/10.5281/zenodo.18623601.

Code availability

The computer codes for analyzing data and drawing plots are developed in NCAR Command Language (available at https://www.ncl.ucar.edu/). The computer codes used in this study are available in the Zenodo repository https://doi.org/10.5281/zenodo.18623601.

References

1. Cohen, J. et al. Recent arctic amplification and extreme mid-latitude weather. *Nat. Geosci.* **7**, 627–637 (2014).

2. Mori, M. et al. A reconciled estimate of the influence of Arctic sea-ice loss on recent Eurasian cooling. *Nat. Clim. Change* **9**, 123–219 (2019).

3. Yin, M. et al. Amplified wintertime Arctic warming causes Eurasian cooling via nonlinear feedback of suppressed synoptic eddy activities. *Sci. Adv.* **11(12)**, eadr6336 (2025).

4. Cohen, J. et al. Divergent consensuses on Arctic amplification influence on midlatitude severe winter weather. *Nat. Clim. Change*, **10**, 20–29 (2020).

5. Gong, H. et al. Teleconnection from Arctic warming suppresses long-term warming in central Eurasia. *Sci. Adv.* **11(4)**, eadq9461 (2025).

6. Yin, Z. C. et al. Subseasonal variability and the "Arctic warming-Eurasia cooling" trend. *Sci. Bull.* **68 (5)**, 528–535 (2023).

7. Blackport, R. & Screen, J. Weakened evidence for mid-latitude impacts of Arctic warming. *Nat. Clim. Change* **10**, 105–106 (2020).

8. Outten, S.D. & Esau, I. A link between Arctic sea ice and recent cooling trends over Eurasia. *Climatic Change* **110**, 1069–1075 (2012).

9. Yang, H. & Fan, K. The Causes of intraseasonal alternating warm and cold variations over China in winter 2021/22. *J. Climate* **37**, 5153–5170 (2024).

10. Yin, Z. C. et al. Why super sandstorm 2021 in North China? *Natl. Sci. Rev.* **9(3)**, nwab165 (2022).

11. Kug, J. et al. Two distinct influences of Arctic warming on cold winters over North America and East Asia. *Nat. Geosci.* **8(10)**, 759–762 (2015).

12. Mori, M. et al. Robust Arctic sea-ice influence to frequent Eurasian cold winters in the recent past. *Nat. Geosci.* **7**, 869–873 (2014).

13. Matsumura, S. & Kosaka, Y. Arctic–Eurasian climate linkage induced by tropical ocean variability. *Nat. Commun.* **10**, 3441 (2019).

14. Luo, B. et al. Decadal variability of winter warm Arctic-cold Eurasia dipole patterns modulated by Pacific Decadal Oscillation and Atlantic Multidecadal Oscillation. *Earths Future* **10**, e2021EF002351 (2022).

15. Mitchell, D. M. et al. The influence of stratospheric vortex displacements and splits on surface climate. *J. Climate* **26**, 2668–2682 (2013).

16. He, S. et al. Eurasian cooling linked to the vertical distribution of Arctic warming. *Geophy. Res. Lett.* **47**, e2020GL087212 (2020).

17. Xu, X. et al. Atmospheric contributions to the reversal of surface temperature anomalies between early and late winter over Eurasia. *Earths Future* **10**, e2022EF002790 (2022).

18. Kidston, J. et al. Stratospheric influence on tropospheric jet streams, storm tracks and surface weather. *Nat. Geosci.* **8(6)**, 433–440 (2015).

19. Shaw, T. A., Perlwitz, J. & Harnik, N. Downward wave coupling between the stratosphere and troposphere: The importance of meridional wave guiding and comparison with zonal-mean coupling. *J. Climate* **23**, 6365–6381 (2010).

20. Baldwin, M. P. et al. Sudden Stratospheric Warmings. *Rev. Geophys.* **59(1)**, e2020RG000708 (2021).

21. Ding, X. et al. Extreme stratospheric wave activity as harbingers of cold events over North America. *Commun. Earth Environ.* **4(1)**, 187 (2023).

22. Davini, P., Cagnazzo C. & Anstey, J. A. A blocking view of the stratosphere-troposphere coupling. *J. Geophys. Res. Atmos.* **119**, 11100–11115 (2014).

23. Chen, Q., Xu, L. & Cai, H. Impact of stratospheric sudden warming on East Asian winter monsoons. *Adv. Meteorol.* **2015**, 640912, (2015)

24. Kolstad, E. W., Breiteig, T., & Scaife, A. A. The association between stratospheric weak polar vortex events and cold air outbreaks in the Northern Hemisphere. *Q. J. R. Meteorol. Soc.* **136(649)**, 886–893 (2010).

25. Kretschmer, M., et al. More-persistent weak stratospheric polar vortex states linked to cold extremes. *Bull. Am. Meteorol. Soc.* **99(1)**, 49–60 (2018).

26. Zou, C. et al. Contrasting physical mechanisms linking stratospheric polar vortex stretching events to cold Eurasia between autumn and late winter. *Clim. Dyn.* **62,** 2399–2417 (2024).

27. Hu, D. et al. Longer duration of extreme cold events over east Asia affected by the stratospheric polar

vortex extension. *J. Geophys. Res. Atmos.* **130**, e2024JD042299 (2025).

28. Domeisen, D. I. V. et al. The role of the stratosphere in subseasonal to seasonal prediction: 2. Predictability arising from stratosphere-troposphere coupling. *J. Geophys. Res. Atmos.*, **125(2)**, e2019JD030923 (2020).

29. Zhang, M., Yang, X. Y. & Huang, Y. Impacts of sudden stratospheric warming on extreme cold events in early 2021: Anensemble-based sensitivity analysis. *Geophys. Res. Lett.* **49**, e2021GL096840 (2022).

30. Shan, Q. & Fan, K. The transition of stratospheric polar vortex intensity: A case study of winter 1987/88. *J. Geophys. Res. Atmos.* **127**, e2022JD036511 (2022).

31. Zhang, C. et al. Impacts of stratospheric polar vortex shift on the East Asian trough. *J. Climate* **35(17)**, 5605–5621 (2022).

32. Karami, H., Jacobi, C. & Kumar, A. The morphology of the stratospheric polar vortex under stratospheric aerosol intervention scenarios. *Int. J. Climatol*. **45(8)**, e8838 (2025).

33. Qian, C. et al. Impacts of the Arctic stratospheric polar vortex weakening on Ural blocking in boreal winter. *J. Geophys. Res. Atmos.* **129**, e2024JD041362 (2024).

34. Song, L., Wu, R. & Jiao, Y. Relative contributions of synoptic and intraseasonal variations to strong cold events over eastern China. *Clim. Dyn.* **50**, 4619–4634 (2018).

35. Domeisen, D. I. V., Sun, L. & Chen G. The role of synoptic eddies in the tropospheric response to stratospheric variability. *Geophys. Res. Lett.* **40**, 4933–4937 (2013)

36. Kurihara, K. & Kawahara, M. Extremes of East Asian weather during the post ENSO years of 1983/84. *J. Meteorol. Soc. Japan* **64**, 493–503 (1986).

37. Kidston, J. et al. Stratospheric influence on tropospheric jet streams, storm tracks and surface weather. *Nat. Geosci.* **8(6)**, 433–440 (2015).

38. Kretschmer, M. et al. The different stratospheric influence on cold-extremes in Eurasia and North America. *npj Clim. Atmo. Sci.* **1**, 44 (2018).

39. Rao, J. et al. Mean state of the Northern Hemisphere stratospheric polar vortex in three generations of CMIP Models. *J. Climate* **35**, 4603–4625 (2022).

40. Domeisen, D. I. V. et al. The role of the stratosphere in subseasonal to seasonal prediction: 1. Predictability of the stratosphere. *J. Geophys. Res. Atmos.* **125(2)**, e2019JD030920 (2019).

41. Polvani, L. M., & Waugh, D. W. Upward wave activity flux as a precursor to extreme stratospheric events and subsequent anomalous surface weather regimes. *J. Climate* **17(18)**, 3548–3554 (2004).

42. Castanheira, J. M., & Barriopedro, D. Dynamical connection between tropospheric blockings and stratospheric polar vortex. *Geophys. Res. Lett.* **37(13)**, L13809 (2010).

43. Kim, B.-M. et al. Weakening of the stratospheric polar vortex by Arctic sea-ice loss. *Nat. Commun.* **5(1)**, 4646 (2014).

44. Cohen, J. et al. Linking Siberian snow cover to precursors of stratospheric variability. *J. Climate* **27(14)**, 5422–5432 (2014).

45. Domeisen, D. I. V., Garfinkel, C. I. & Butler, A. H. The teleconnection of El Niño southern oscillation to the stratosphere. *Rev. Geophys.* **57(1)**, 5–47 (2019).

46. Fan, K., Yang, H. & Dai, H. Research progress on inter-monthly winter temperature variation in East Asia and climate prediction. *Atmos. Oceanic Sci. Lett.* **16**, 100372 (2023)

47. Tian, W. et al. Role of Stratospheric Processes in Climate Change: Advances and Challenges. *Adv. Atmos. Sci.* **40**, 1379–1400 (2023).

48. Meng, J. et al. Arctic weather variability and connectivity. *Nat. Commun.* **14**, 6574 (2023).

49. Huang, J. et al. Stratospheric influence on the development of the 2018 late winter European cold air outbreak. *J. Geophys. Res. Atmos.* **127**, e2021JD035877 (2022).

50. Xu, T. et al. Hybrid seasonal prediction of meridional temperature gradient associated with "Warm Arctic-Cold Eurasia". *Adv. Atmos. Sci.* **40(9)**, 1649–1661 (2023).

51. Yin, Z. et al. Traditional Meiyu-Baiu has been suspended by global warming, *Natl. Sci. Rev.* **11(7)**, nwae166 (2024).

52. Hersbach, H. et al. ERA5 hourly data on single levels from 1940 to present. Copernicus Climate Change Service (C3S) Climate Data Store (CDS) (2023).

53. Wilks, D. S. Statistical Methods in the Atmospheric Sciences 3rd edn. (Academic Press, 2011).

54. Liang, X. S. Unraveling the cause-effect relation between time series. *Phys. Rev.* **90(5)**, 052150 (2014).

55. Ma, J. et al. Skillful seasonal predictions of continental East-Asian summer rainfall by integrating its spatio-temporal evolution. *Nat. Commun.* **16**, 273 (2025).

56. Plumb, R. A. On the three-dimensional propagation of stationary waves. *J. Atmos. Sci.* **42**, 217–229 (1985).

57. Ren, H. et al. Dynamic synoptic eddy feedbacks contributing to maintenance and propagation of intraseasonal NAO. *Geophys. Res. Lett.* **49**, e2021GL096508 (2022)

58. Zhang, R. et al. A stratospheric precursor of East Asian summer droughts and floods. *Nat. Commun.* **15**, 247 (2024).

59. Eyring, V. et al. Overview of the Coupled Model Intercomparison Project Phase 6 (CMIP6) experimental design and organization. *Geosci. Model Dev.* **9**,1937–1958 (2016).

60. Kay, J. E. et al. The Community Earth System Model (CESM) large ensemble project: A community resource for studying climate change in the presence of internal climate variability. *Bull. Am. Meteorol. Soc.* **96(8)**, 1333–1349 (2015).

Acknowledgments

Funding: National Natural Science Foundation of China 42394125 to Z.Y., 42505058 to Y.Z., and the Postdoctoral Fellowship Program of CPSF GZB20250077 to Y.Z.

Author Contributions Statement

Y.Z. and Z.Y. conceived and designed the study; Y.Z., Z.Y. and S.H. performed the analyses; Y.Z. and Z.Y. wrote the draft paper; W.T., S.H. and P.H. helped improve the paper. All authors discussed the results and contributed to writing the paper.

Competing Interests Statement

The authors declare no competing interests.

Figure Captions

Fig. 1. Linkages between the precursory stratospheric polar vortex and the reversal of "warm Arctic-cold Eurasia". Composites of the potential vorticity on the 530K isentropic surface in (a) November 1st to December 15th and (b) December 16th to February 10th in the "warm Arctic-cold Eurasia" (WACE) pattern reversal years during 1979/80 to 2023/24 (cold Arctic-warm Eurasia (CAWE) to WACE years minus WACE to CAWE years). The green, pink and blue lines represent the composited polar vortex edge in climate mean, CAWE to CAWE years and WACE to CAWE years, respectively. The edge of stratospheric polar vortex is determined by 58PVU on the 530K isentropic. The white dots indicate that the results are significant above the 95% confidence level. (c) The upper part: Daily variations of the stratospheric polar vortex morphology over North America-North Atlantic (NANA-SPV_{IPV}; red solid line) and the WACE pattern ($WACE_T$; black solid line) composited in the $WACE_T$ reversal years (CAWE to WACE years minus WACE to CAWE years), and the composited variations after 45-day low-pass filtering are represented by the thick lines. The thicker lines indicate that the results are significant above the 95% confidence level. The red shadings represent the Nov1Dec15 and Dec16Feb10 periods associated with NANA-SPV_{IPV} transitions, and the gray shadings represent the early and late winter associated with $WACE_T$ reversal. The lower part: 45-day moving t-test of the NANA-SPV_{IPV} and $WACE_T$ during November to February in each $WACE_T$ reversal years (shading) and their means (lines), and the most significant point are represented by the markers. The linear trend is removed.

Fig. 2. Responses of the atmospheric circulations and surface air temperature to the stratospheric polar vortex morphology transition over North America-North Atlantic. (a) Composites of the geopotential height at 50 hPa in Nov1Dec15 (the top panel), the geopotential height at 500 hPa in Nov1Dec15 (contours) and in Dec1Jan10 (shadings), the wind at 850 hPa in Dec1Jan10 (arrow, the middle

panel), and the surface air temperature (SAT) in Dec1Jan10 (the bottom panel) according to the transition of stratospheric polar vortex morphology over North America-North Atlantic (NANA-SPV_{IPV}) during 1979/80 to 2023/24 (negative to positive NANA-SPV_{IPV} years minus positive to negative NANA-SPV_{IPV} years). (b) Composites of the geopotential height at 50 hPa in Dec16Feb10 (the top panel), the geopotential height at 500 hPa in Dec16Feb10 (contours) and in Jan11Feb28 (shadings), the wind at 850 hPa in Jan11Feb28 (arrow, the middle panel), and the SAT in Jan11Feb28 (the bottom panel) according to NANA-SPV_{IPV} transition during 1979/80 to 2023/24. The cyan arrows represent the propagation of the Plumb wave at the 500 hPa in Nov1Dec15 and Dec16Feb10. The contours and shadings in the top and middle panels and the white dots in the bottom panels indicate that the results are significant above the 95% confidence level.

Fig. 3. Physical mechanisms of the stratospheric polar vortex morphology transition over North America-North Atlantic impacting the reversal of "warm Arctic-cold Eurasia". Composites of the anomalous geopotential height (shading) and the vertical and zonal components of anomalous Plumb wave activity flux (vector) averaged over 60°–70°N as a function of longitude and pressure in (a) Nov1Dec15 and (b) Dec16Feb10 according to the transition of stratospheric polar vortex morphology over North America-North Atlantic (NANA-SPV_{IPV}) during 1979/80 to 2023/24 (negative to positive NANA-SPV_{IPV} years minus positive to negative NANA-SPV_{IPV} years). The magnitude of the Plumb flux is scaled by $(1000/p)^{1/2}$. (c) Composites of the daily variations of the pressure-temporal geopotential height (shadings) and zonal wind (contours) along 0–120°W, 60–70°N, and the daily variations of NANA-SPV_{IPV}, Ural blocking (UB) and "warm Arctic-cold Eurasia" pattern ($WACE_T$) index according to NANA-SPV_{IPV} transition during 1979/80 to 2023/24 (negative to positive NANA-SPV_{IPV} years minus positive to negative NANA-SPV_{IPV} years). The composited variations after 45-day low-pass filtering are represented by the smooth lines. The thicker lines indicate that the results are significant above the 95% confidence level. The white dots indicate that the results are significant above the 95% confidence level.

Fig. 4. Verifications of the physical linkages in simulations. (a) Multi-member mean and the probability distribution of the simulated difference of "warm Arctic-cold Eurasia" pattern between early and late winter (Diff-$WACE_T$) in the simulated transition of stratospheric polar vortex morphology over North

America-North Atlantic from contraction to stretching (Con-to-Stre NANA-SPV) years (red) and from stretching to contraction (Stre-to-Con NANA-SPV) years (blue) based on CMIP6 simulations and CESM-LE simulations. The center line, box limits and whiskers of the box-plots elements are defined as mean, upper and lower quartiles, maximum and minimum, respectively. The hollow triangles represent the reanalysis results. (b) The simulated "warm Arctic-cold Eurasia" pattern ($WACE_T$) in early and late winter in the simulated Con-to-Stre NANA-SPV years (red) and Stre-to-Con NANA-SPV years (blue) based on the High-top and Low-top CMIP6 models. The center line, box limits and whiskers of the box-plots elements are defined as mean, upper and lower quartiles, maximum and minimum, respectively. (c, d) Composites of the pressure-temporal geopotential height along 0–120°W, 60–75°N, and the daily variation of the geopotential height anomalies at 500 hPa over the North America-North Atlantic ($NANA_{Z500}$), Ural blocking (UB) and $WACE_T$ according to the simulated stratospheric polar vortex morphology transition (Con-to-Stre NANA-SPV years minus Stre-to-Con NANA-SPV years) that selected from the High-top and Low-top CMIP6 models. The white dots and the thicker lines indicate that the results are significant above the 95% confidence level.

Fig. 5. The timeline and physical process of the stratospheric polar vortex morphology transition over North America-North Atlantic modulating the phase reversal of "warm Arctic-cold Eurasia". The contracted stratospheric polar vortex (SPV) over North America-North Atlantic with zonal asymmetric anomalies in Nov1Dec15 causes the suppressed Ural high in early winter through the vertical wave coupling and transmission of the Rossby wave, leading to the cold Arctic-warm Eurasia phase. While in Dec16Feb10, the SPV stretches toward North America-North Atlantic and enhances across the Arctic, causing the sustained Ural blocking in late winter through downward-propagation and synoptic eddy feedback, resulting in the warm Arctic-cold Eurasia phase opposite to that in early winter. The red and blue arrows indicate abnormal anticyclones and cyclones. The dotted arrow indicates the evolution of stratospheric anomalies. The blue and yellow thick lines represent the geopotential height at 500 hPa. The clock indicates the period from November to March, and the red and grey shadows in the clock indicate the duration of the two stages of the SPV morphology and "warm Arctic-cold Eurasia" pattern. The SPV morphology transition leads the phase reversal of "warm Arctic-cold Eurasia" pattern by about 25 days.

Editorial Summary

This study shows that a transition of the stratospheric polar vortex morphology is an effective precursor of the phase reversal of the "warm Arctic-cold Eurasia" pattern in winter and that CMIP6 models with complete stratospheric processes can successfully capture this physical link.

Peer review information: *Nature Communications* thanks the anonymous reviewers for their contribution to the peer review of this work. A peer review file is available.